Ultrafast changes of magnetic anisotropy driven by laser-generated coherent and non-coherent phonons in metallic films

V. N. Kats,[1] T. L. Linnik,[2] A. S. Salasyuk,[1] A. W. Rushforth,[3] M. Wang,[4] P. Wadley,[3] A.V. Akimov,[3] S. A. Cavill,[5] V. Holy,[6] A. M. Kalashnikova,[1] and A. V. Scherbakov[1]

Affiliations

[1]*Ioffe Physical-Technical Institute, Russian Academy of Sciences, 194021 St. Petersburg, Russia*

[2]*Department of Theoretical Physics, V.E. Lashkaryov Institute of Semiconductor Physics, 03028 Kyiv, Ukraine*

[3]*School of Physics and Astronomy, University of Nottingham, Nottingham NG7 2RD, United Kingdom*

[4]*London Centre for Nanotechnology, University College London, 17-19 Gordon Street, London WC1H 0AH, United Kingdom*

[5]*Department of Physics, University of York, Heslington, York, YO10 5DD, United Kingdom*

[6]*Faculty of Mathematics and Physics, Charles University in Prague, Ke Karlovu 3, 121 16 Prague 2, Czech Republic.*

ABSTRACT

Ultrafast optical excitation of a metal ferromagnetic film results in a modification of the magneto-crystalline anisotropy and induces the magnetization precession. We consider two main contributions to these processes: an effect of non-coherent phonons, which modifies the temperature dependent parameters of the magneto-crystalline anisotropy; and coherent phonons in the form of a strain contributing via inverse magnetostriction. Contrary to the earlier experiments with high symmetry ferromagnetic structures, where these mechanisms could not be separated, we study the magnetization response to femtosecond optical pulses in the low-symmetry magnetostrictive Galfenol film so that it is possible to separate the coherent and non-coherent phonon contributions. By choosing certain experimental geometry and external magnetic field, we can distinguish the contribution from a specific mechanism. Theoretical analysis and numerical calculations are used to support the experimental observations and proposed model.

1. Introduction

Since the first experiments on ultrafast demagnetization in Ni [1] femtosecond light pulses have been continuously developing as a tool to manipulate magnetic order on the ultrashort time scales. The response of magnetization to femtosecond optical excitation has been widely studied in various magnetically ordered materials [2] and attracts a significant attention nowadays. The particular interest is related to ultrafast magnetization dynamics in metals, stimulated by expectations of technological breakthrough in computing, data processing and data storage if optical control is implemented into magnetic applications. A promising example is a drastically increased magnetic data storage capacity provided by the technology of heat-assisted magnetic recording [3]. The all-optical switching of magnetization demonstrated recently in ferrimagnetic single phase [4] and multilayered [5] metallic structures may push also the magnetic applications to the time scales, which have been inaccessible previously.

Among various phenomena resulting from the ultrafast laser excitation of ferromagnets, changes in the magneto-crystalline anisotropy (MCA) parameters play a crucial role. The typical manifestation of this phenomenon is triggering the magnetization precession, and this can be conveniently monitored directly in the time-domain [6]. At equilibrium, the magnetization **M** is aligned parallel to the effective field $\mathbf{B}_{\mathbf{eff}}$, which comprises the MCA, and external magnetic field **B**. The femtosecond laser pulse modifies the MCA and, thus, tilts the direction of $\mathbf{B}_{\mathbf{eff}}$. The time required for the alignment of magnetization **M** along the new direction is much longer than the transient kinetics of the effective field. Thus, immediately after the laser excitation **M** becomes unparallel to $\mathbf{B}_{\mathbf{eff}}$ and relaxes to the new direction precessionally. This precession with a frequency equal to the frequency of the ferromagnetic resonance persists until **M** relaxes toward the new quasi-equilibrium orientation of $\mathbf{B}_{\mathbf{eff}}$.

Whilst the phenomenological scenario of the laser induced precessional response due to the ultrafast MCA changes is clear, the specific physical mechanisms of optically excited precessional dynamics in a ferromagnet are under debate. In ferromagnetic metals the laser pulse penetrates to a depth of ~10 nm where the absorption of light ultimately results in the emission of phonons, i.e. lattice heating. Due to electron-phonon interaction this process takes place on sub-picosecond time scale and often may be considered as an instantaneous rise of the lattice temperature *T*. The increase of *T* affects the values of the MCA parameters and $\mathbf{B}_{\mathbf{eff}}$ tilts from its equilibrium position. Such a scenario has been considered in a number of previous works and may be attributed to the modulation of MCA by *non-coherent phonons* generated as a result of optical excitation [7-11].

In addition, the instantaneous rise of T in a thin layer of ferromagnetic metal results in the generation of thermal stress in a near-surface region. This thermal stress induces strain of two forms: persistent anisotropic quasi-uniform strain, and picosecond strain pulses propagating away from the surface with sound velocities, which both may be considered as wavepackets of *coherent phonons* [12]. The strain-induced changes of the MCA (i.e. inverse magnetostriction effect) first were discussed in Ref. [13] as a possible impact for triggering the magnetization precession. Later, coherent phonons have been shown to be an efficient stimulus for changing the MCA in experiments with picosecond strain pulses, when the magnetization precession is excited without direct optical excitation of the ferromagnet [14,15], and with optically excited surface acoustic waves [16,17]. In these experiments, the amplitude of the precession was large enough that we can assume that the coherent phonons may also have a significant contribution when the metal ferromagnet is excited directly by an optical pulse. However, it has been difficult to pick out the contributions from coherent and non-coherent phonons separately because the generation of strain is inseparable from the temperature rise in the experiments with optically excited ferromagnetic metals. Coherent and non-coherent phonon mechanisms in metals have been modeled separately in Ref. [14,15] and Ref. [7-11] respectively, but there is no way to compare quantitatively the contributions of these mechanisms to changes of the MCA as a result of direct optical excitation.

The aim of the present work is to distinguish quantitatively the role of coherent and non-coherent phonons in experiments where changes in the MCA parameters and subsequent magnetization precession are induced by direct optical excitation of a metal ferromagnetic film. Contrary to earlier works [7-11,13,18,19], where the optically induced precession was studied, we use a ferromagnetic film with low symmetry orientation. It is important that we use the experimental geometry, which allows us to exclude the ultrafast demagnetization as a stimulus for the excitation of magnetization precession [7,18,19] leaving only the changes of MCA as the main mechanisms for launching the precession. We demonstrate that the B-dependencies of the amplitude and phase of the precession are very different for coherent and non-coherent phonon mechanisms. Comparing the results of the experiments with the theoretical simulations, we demonstrate that the coherent phonon mechanism may dominate over the non-coherent mechanism in a ferromagnetic film with strong magneto-elastic coupling and specific MCA for a certain film orientation and value of B.

We study a film of Galfenol, which is a novel ferromagnetic alloy of Iron and Gallium of high technological potential [20,21]. The combination of enhanced magnetostriction, high saturation magnetization of 1.8 T and low saturation field with technological accessibility makes Galfenol attractive for nanoscale magnetostrictive applications [21], e.g. strain-assisted control of

magnetization by electric field [22]. In the experiments with picosecond stain pulses injected into a Galfenol film from a GaAs substrate, the strain effectively triggers high-amplitude magnetization precession [15]. However, direct optical excitation of magnetization dynamics of Galfenol has not been studied so far and the comparative role of coherent and non-coherent phonons in the changes of the MCA remains unexplored. In our study, we use the low symmetry Galfenol film grown on (311)-GaAs substrate. We shall show that the choice of low symmetry orientation allows us to pick out the contribution of a particular mechanism for modulation of MCA.

The paper consists of four main parts. In Section 2, we describe the samples under study and the experimental technique. Section 3 is devoted to the experimental results on the laser-induced magnetization precession in the low-symmetry Galfenol film. Section 4 presents the discussion, theoretical analysis and numerical calculations. In Section 5, we compare experimental and numerical results for low- and high-symmetry Galfenol structures.

2. Experimental technique

The sample under study is a Galfenol film ($Fe_{0.81}Ga_{0.19}$) of 100-nm thickness grown by magnetron sputtering on a (311)-GaAs substrate. The film plane is formed by two orthogonal crystallographic directions, $[\bar{2}33]$ and $[0\bar{1}1]$, which are referred to further as the *x*-axis and *y*-axes, respectively [see Fig. 1(a)]. Detailed X-ray characterization showed that the film is a mosaic structure formed from crystallites, each possessing a cubic crystal structure. The random root-mean square misorientation of the crystallites is few degrees. Therefore, in the following discussion we treat magneto-crystalline and elastic anisotropies of this structure as those for a single crystalline film. Superconducting quantum interference device (SQUID) measurements confirm the pronounced MCA of the studied film, with the easy axis lying in the sample plane close to $[0\bar{1}1]$ direction (*y*-axis). As a reference, we also studied the laser-induced magnetization dynamics in a Galfenol film of the same composition grown on a (001)-GaAs substrate.

In order to study experimentally the ultrafast modulation of the MCA we measure the precessional response of the magnetization to femtosecond optical excitation employing a conventional time-resolved magneto-optical Kerr effect technique (TRMOKE) shown schematically in Fig. 1(b). A Yb:KGW regenerative amplifier generates laser pulses at the central wavelength of 1030 nm with the duration of 190 fs and the repetition rate of 5 kHz. The pump pulses of the energy density, *P*, of 2÷20 mJ/cm^2 focused in the spot of Gaussian shape of 150-μm diameter (full width at half maximum) were used for exciting the Galfenol film. The linearly

polarized probe pulse split from the same laser source was focused onto the excited area at the front side of the film. The energy density of the probe pulse was 10 μJ/cm^2 in the focusing spot of 100-μm diameter. The incident angles for both pulses were several degrees with respect to the surface normal. We monitored the change of the out-of plane component of magnetization, M_z, by measuring the rotation of the probe polarization due to the polar magneto-optical Kerr effect as a function of the time delay between the pump and probe pulses provided by a variable delay line with up to 100-fs time resolution. An external magnetic field **B** was applied in the plane of the film at various angles with respect to the *x*-axis. All measurements were performed at room temperature.

3. Experimental results

Figures 1(c) and 1(d) show the pump-induced changes of the Kerr rotations of the probe pulse polarization as a function of the pump-probe time-delay measured at various values of the external magnetic field *B*, applied in the film plane along the *x*-axis. We demonstrate the signals and dependences measured at *P*=10 mJ/cm2, since this value provides reasonable signal to noise ratio with no sign of non-linearity. The signals measured at lower or higher excitation densities are similar with the linearly decreased or increased amplitudes respectively. The signal demonstrates pronounced oscillations, which start at *t*=0, corresponding to the excitation of the film by the pump pulse, and decay within 500 ps. Figure 1(e) shows the spectra for the measured signals obtained as their fast Fourier transforms (FFTs). The spectra consist of a single spectral line and its position and amplitude clearly changes with *B*. At **B**||y we observe no excitation of the magnetization precession. This and the intermediate field orientations are not shown in Fig. 2 because they do not provide any additional information. We ascribe the oscillations in the TRMOKE signal to the modulation of the normal component $M_z(t)$ of the magnetization due to its precessional motion induced by the pump pulses.

There are four main parameters of the magnetization precession: frequency, *f*, amplitude, $\Delta M_z^{\max}$, initial phase, ψ_0, and decay time, τ_M, which characterize the response of **M** to the optically induced changes of the MCA. In order to perform comprehensive analysis, we have measured two types of signals for each value of *B*: 2-ps time resolution signals in long 1-ns time interval [Fig 1(c)]; and 200-fs time resolution signals in the time intervals covering the first few oscillation periods [Fig. 1(d)]. These measurements allowed us to obtain the precise values for *f*, $\Delta M_z^{\max}$, ψ_0, and τ_M by fitting the experimental curves with the expression

$$\Delta M_z(t) = \Delta M_z^{\max} \exp\left(-\frac{t}{\tau_M}\right)\sin(2\pi f t - \psi_0) + Y_0, \qquad (1)$$

where the parameter Y_0 serves to describe the long-living background in the TRMOKE signal, which reflects the changes of magneto-optical properties of the film under intense optical excitation, but does not relate directly to the magnetization precession. We determine the starting time t=0 by the appearance of a sharp high-intensity peak in the high-resolution signal [see Fig. 1(d)]. This peak is observed at all values of B at the same position of the delay line.

Figure 2 summarizes the B-dependences of the precession parameters extracted from the fit. The dependencies of precession frequency $f(B)$, amplitude $\Delta M_z^{\max}(B)$ and phase $\psi_0(B)$ are shown in Figs. 2(a), 2(b) and 2(c), respectively. The decay time τ_M has been found to be independent of B in the considered field range and $\tau_M \approx 100$ ps, which is in good agreement with our previous results [15]. The precession parameters shown in Fig. 2 possess nonmonotonic B-dependences with the pronounced extrema at B=150 mT. The dependences of $f(B)$ and $\Delta M_z^{\max}(B)$ are typical for magnetization precession in low- and high-symmetry ferromagnetic films when the external magnetic field is applied along the hard magnetization axes [8,15]. However, the strong dependence of the precession phase $\psi_0(B)$ on magnetic field is a new and very important experimental observation. At low fields, B<150 mT, the phase rapidly decreases down to $\psi_0=0$, and then gradually increases up towards $\psi_0=\pi/2$. In the theoretical analysis presented in the next section, the dependences of $\Delta M_z^{\max}(B)$ and $\psi_0(B)$ will allow us to distinguish the contributions from coherent and non-coherent phonons to the changes of MCA.

4. Theoretical analysis and discussion.

In accordance with the model proposed by van Kampen et al. [18] and followed by a number of works [7-11,19], we assume that the femtosecond laser pulse launches the magnetization precession by modifying the magnetic anisotropy and, thus, tilting the effective magnetic field $\mathbf{B_{eff}}$. In ferromagnetic Galfenol the absorbed energy transfer from the optical excitation to non-coherent phonons results in a rapid lattice temperature rise and changes in the MCA parameters due to their temperature dependence [23]. The temperature rise also produces thermal stress due to the thermal expansion. This instantaneously generated stress leads to generation of coherent phonons [12]. The generation of the coherent phonons is confirmed by the transient reflectivity measurements, which demonstrate oscillating signal (i.e. Brillouin oscillation) with two frequencies of 34.8 and 19.8 GHz due to the dynamical interference of the probe beam at the propagating strain pulses [24]. These frequencies are independent of the applied magnetic field and correspond to the quasi-longitudinal (QLA) and quasi-transverse (QTA) acoustic modes, respectively, in agreement with

our previous observations and analysis [25]. The coherent phonons modify the MCA via inverse magnetostriction [15,22]. The transient changes of the MCA are supposed to be much faster (<10 ps) than the characteristic times (the precession period and decay time) of the precession kinetics [1,2]. Thus, we may consider the time dependence of the tilt of $\mathbf{B}_{\mathbf{eff}}$ to an altered orientation as a step-like function. The following relaxation time to the equilibrium state (~10 ns) is much longer than the precession decay time and we may assume that $\mathbf{B}_{\mathbf{eff}}$ remains in the altered position for the whole time range while monitoring the magnetization precession. Thus, the precession parameters, which we extract from the TRMOKE signals, are determined by $\mathbf{B}_{\mathbf{eff}}$ and its tilt out of the initial (equilibrium) orientation.

We model the magnetization response using the Landau-Lifshitz equation for precession around the time-dependent effective field $\mathbf{B}_{\mathrm{eff}}$:

$$\frac{d\mathbf{m}}{dt} = -\gamma \cdot \mathbf{m} \times \mathbf{B}_{\mathbf{eff}}(\mathbf{m},t), \qquad \mathbf{B}_{\mathbf{eff}}(\mathbf{m},t) = -\nabla_{\mathbf{m}} F_M(\mathbf{m},t), \tag{2}$$

where $\mathbf{m} = \mathbf{M}/M_S$ is the normalized magnetization, $\gamma = g\mu_B/\hbar$ (g=2 is g-factor, μ_B is Bohr magneton and $\hbar$ is Plank constant) is the gyromagnetic ratio, and the effective field $\mathbf{B}_{\mathbf{eff}}$ is introduced as the gradient of the normalized free energy density of the ferromagnetic layer $F_M = F/M_S$. The general expression for F_M of a thin layer of ferromagnetic material with cubic symmetry may be written in the form [26-28]:

$$\begin{aligned} F_M(\mathbf{m}) = &-(\mathbf{m}\cdot\mathbf{B}) + B_d m_z^2 + K_1(m_{x'}^2 m_{y'}^2 + m_{z'}^2 m_{y'}^2 + m_{x'}^2 m_{z'}^2) - K_u(\mathbf{m}\cdot\mathbf{s})^2 + \\ &+ b_1\left(\varepsilon_{x'x'} m_{x'}^2 + \varepsilon_{y'y'} m_{y'}^2 + \varepsilon_{z'z'} m_{z'}^2\right) + b_2(\varepsilon_{x'y'} m_{x'} m_{y'} + \varepsilon_{x'z'} m_{x'} m_{z'} + \varepsilon_{y'z'} m_{y'} m_{z'}) \end{aligned}, \tag{3}$$

where m_x, m_y, m_z and $m_{x'}$, m_y, $m_{z'}$ are the projections of **m** onto the [311] and cubic coordinate axes, respectively, in accordance with the scheme shown in Fig. 1 (a), and **s** is the unit vector along the uniaxial anisotropy direction. The first term in Eq. (3) is the Zeeman energy of **m** in the external magnetic field **B**. The second term is the demagnetization energy in the demagnetizing field $B_d = \mu_o M_S/2$. The following two terms describe the cubic anisotropy and uniaxial anisotropy through the anisotropy coefficients K_1 and K_u. The magneto-elastic energy of a strained cubic ferromagnet is given by last two terms through the magneto-elastic coefficients b_1 and b_2 and the strain components $\varepsilon_{l,n}$ ($l,n=x',y',z'$) in cubic coordinate axes. The values of B_d, K_1 and K_u determine the equilibrium orientation of magnetization, which corresponds to the minimum of the free energy density F_M. The magneto-elastic part of F_M is zero in the unstrained lattice, but becomes contributing to F_M in the optically excited film due to the thermal stress. In general, the strain

components in Eq. (3) include both contributions: the persistent strain indicated below as $\Delta\varepsilon_{ij}$, and the strain pulses.

In order to get all the anisotropy parameters, we have analyzed the data published for (Fe,Ga) alloys and take the parameters for concentration of Ga atoms equal to 19% as M_0=1.59 T, b_1= -6 T, b_2=2 T [29] and cubic anisotropy K_1=30 mT [21,30]. As there is not enough data on the uniaxial anisotropy direction in (311)-FeGa/GaAs films we choose initially in Eq. (3) $\mathbf{s} \parallel [0\bar{1}1]$. Then from the data for the films on GaAs substrates of different symmetries in combination with the fitting of our experimental frequency dependences on magnetic field we obtain the value K_u=45 mT. This value of K_u results in the easy magnetization axis along $[0\bar{1}1]$ crystallographic direction in accordance with the SQUID measurements.

First, we calculate the equilibrium orientation of the effective magnetic field $\mathbf{B_{eff}}$ at different values of the applied magnetic field $\mathbf{B}\|$x. Figure 3(a) shows the B-dependence of the equilibrium orientation of $\mathbf{B_{eff}}$ and, respectively, **M** in the absence of optical excitation. At B=0, $\mathbf{B_{eff}}$ lies along the easy axis close to the $[0\bar{1}1]$ direction (y-axis). With the increase of B, $\mathbf{B_{eff}}$ gradually turns towards the external field direction remaining in the film plane and becomes parallel to $[\bar{2}33]$ (x-axis) at B≈150 mT.

In the linear approximation, the precession frequency is determined by the equilibrium $\mathbf{B_{eff}}$, and we can calculate the field dependence $f(B)$ using a standard ferromagnetic resonance formalism [31]. The solid line in Fig. 2 (a) shows the calculated $f(B)$ dependence for the described film parameters. It demonstrates very good quantitative agreement with the experimental results. We have to introduce a small (1 degree) deviation of external magnetic field from the $[\bar{2}33]$ direction in order to get the best agreement around B≈150 mT. In the case of external magnetic field perfectly aligned along the $[\bar{2}33]$ direction, $f(B)$ should go through zero at the field when $\mathbf{B_{eff}}$ switches to the hard axis. The 1-degree deviation of B is within the accuracy of the experimental setup and results in finite f at this value of B.

The amplitude $\Delta M_z^{\max}$ and initial phase ψ_0 of the precession are determined by the tilt of $\mathbf{B_{eff}}$, from its equilibrium position due to the optically altered magnetic anisotropy. The optical altering includes generation of the optically induced strain [12] (coherent phonon mechanism), which contributes through magneto-elastic energy terms, and changes of the lattice temperature-dependent coefficients K_1 and K_u [23] (non-coherent phonon mechanism). For the optical excitation density P=10 mJ/cm^2, we get the temperature increase of 120 K. This value is set over the film depth within ≈10 ps after the optical excitation due to electron thermal diffusion from the

near-surface region and energy transfer to the lattice [32,33] (see Appendix A) This temperature rise in the (311)-metal film results in the generation of strain with two polarization components [25]: compressive $\varepsilon_{zz}=\Delta\varepsilon_{zz}=1.2\times10^{-3}$ and shear $\varepsilon_{xz}=\Delta\varepsilon_{xz}=-4\times10^{-4}$ (the contribution of the strain pulses is neglected). They may be converted to the cubic coordinate system *x'y'z'* used in Eq. (3) by a standard coordinate frame rotation procedure. The temperature induced changes of K_1 and K_u may be found by fitting the experimental data of $\Delta M_z^{\max}(B)$ [Fig. 2(b)] and we get the best agreement when ΔK_1 = -4.75 mT and ΔK_u =-2.2 mT, respectively (Appendix B). Since at the equilibrium orientation **M** lies in the film plane (m_z=0), the ultrafast demagnetization and respective decrease of the demagnetizing field B_d do not contribute directly to the excitation of magnetization precession. Contrary to the experiments with the out-of-plane orientation of external magnetic field [7,18,19], in the used experimental geometry, the decrease of B_d may result only in non-linear effects, which are not observed in our experiments at all used excitation densities. Thus, we exclude the ultrafast demagnetization as a contributing mechanism from the following consideration.

By minimizing the free energy with modified anisotropy parameters, we have calculated the altered orientation of $\mathbf{B_{eff}}$. Figure 3 (b) shows the results of the calculation when non-coherent and coherent phonon mechanisms are considered separately. The non-coherent phonon mechanism can be modeled by introducing changes in the parameters K_1 and K_u in the Eq. (3) for the free energy density at zero strain. For modeling the coherent phonon mechanism for altering $\mathbf{B_{eff}}$ we keep values K_1 and K_u unperturbed and take into account only the strain-induced changes in the MCA. Figure 3 (b) shows *B*-dependencies of the in- and out-of- plane tilt angles for $\mathbf{B_{eff}}$ which are labeled $\Delta\varphi$ and $\Delta\theta$ respectively, as shown in the inset of Fig.3 (b). The *B*-dependences are presented in logarithmic scale because of an order of magnitude difference in maximal values of $\Delta\varphi$ and $\Delta\theta$. It is clearly seen that, the temperature rise (non-coherent phonon mechanism) turns $\mathbf{B_{eff}}$ out of equilibrium orientation keeping it mainly in the plane of the film in the whole range of *B* because $\Delta\varphi$ shown by solid red line is much larger the $\Delta\theta$ marked by dashed red line in Fig. 3 (b). The coherent phonon mechanism alters $\mathbf{B_{eff}}$ in a more complex way with the in-plane and out-of-plane tilts dominating in different field ranges [see blue lines in Fig 3 (b)]. At low *B*<150 mT we see the mixed behavior induced by both non-coherent and coherent phonon mechanisms. At *B*≈150 mT the non-coherent phonon mechanism is dominant and inducing the in-plane tilt of $\mathbf{B_{eff}}$. With the increase of *B* the coherent phonon mechanism takes over the non-coherent one. Thus, the theoretical analysis for Galfenol film in the considered geometry shows that the non-coherent phonon mechanism for tilting $\mathbf{B_{eff}}$ is dominant at low *B* and coherent phonons give larger contribution to the tilt at high *B* respectively.

The net tilt $\eta = \sqrt{\Delta\varphi^2 + \Delta\theta^2}$ of $\mathbf{B}_{\mathbf{eff}}$ induced by coherent and non-coherent phonons is shown as a function of *B* by the short-dashed line in Fig. 3(b). This curve characterizes the amplitude of the magnetization precession $\Delta M_z^{\max}(B)$ while the initial phase $\psi_0(B)$ of the precession reflects the ratio of in- and out-of-plane tilt angles. For instance, at *B*=150 mT, when $\Delta\varphi >> \Delta\theta$ and the non-coherent phonon mechanism is dominant, we get $\psi_0 \approx 0$. In contrast, at high *B*≈500 mT when the coherent phonon mechanism gives a major contribution and $\Delta\theta >> \Delta\varphi$, we get $\psi_0 \approx \pi/2$. The theoretical analysis with analytical solution, which explains such a dependence of the precession phase, is given in Appendix B. Briefly, there is zero in-plane tilt of $\mathbf{B}_{\mathbf{eff}}$ due to either coherent or non-coherent phonon mechanisms if $\mathbf{B}_{\mathbf{eff}}$ is parallel to the *x*-axis. The out-of-plane tilt remains nonzero at this orientation due to the low symmetry of the studied structure. However, at $\varphi \approx 0$ the contribution of non-coherent phonons becomes minimal, while the coherent phonon mechanism, contrary, achieves its maximal efficiency. The calculated *B*-dependences $\Delta M_z^{\max}(B)$ and $\psi_0(B)$ are shown together with the experimental data in Figs. 2 (b) and 2(c) by solid lines. We point out good agreement between the experimental results and numerical modeling. Here we also see that around *B*=150 mT the non-coherent mechanism dominates and determines the initial precession phase, while at higher fields the out-of-plane phase of precession is determined by the dominating coherent mechanism. It is important to note, that the experimental ratio of the precession amplitudes at *B*=150 and 500 mT [Fig. 2 (b)] is a factor of 4 which is much less than the calculated ratio >10 for η at the same values of *B* [see short-dashed line in Fig. 3 (b)]. This difference is due to the strongly elliptical precession trajectory of **M** due to the demagnetizing factor if the precession axis lies in the film plane.

5. High-symmetry case

For generalizing the obtained results, it is instructive to compare results discussed above with the case when the magnetization precession is excited in the high-symmetry (001)-Galfenol film. We have carried out the TRMOKE measurements in the $Fe_{0.81}Ga_{0.19}$ film of 100-nm thickness grown on a (001)-GaAs substrate. The film is characterized by cubic anisotropy with the in-plane uniaxial distortion, which is known to turn the easy axis of magnetization towards the [110] crystallographic direction ($\mathbf{s} \parallel [110]$)[21]. In the experiments we have observed the optically excited magnetization precession when **B** is not parallel to [110] -direction. Here we present the results obtained for **B**||[100] as the most suitable case for the theoretical analysis. Fig. 4 shows the *B*-dependences of frequency, amplitude and phase of the magnetization precession. As can be seen

in Fig. 4 (a) f increases with B almost linearly, $\Delta M_z^{max}(B)$ demonstrates a broad maximum around B=200 mT [Fig, 4 (b)], and the precession phase ψ_0 is close to 0 in the whole range of B [Fig, 4 (c)]. For the theoretical calculations we used the following anisotropy parameters K_1=30 mT, K_u=70 mT and their changes due to the 120 K temperature increase: ΔK_1=-4.25 mT and ΔK_u=-8.25 mT, respectively. The cubic anisotropy parameter and its changes are assumed the same as in the (311)-film, but the uniaxial term is slightly higher. In contrast to the (311)-film, the strain generated as a result of optical excitation has only one nonzero component $\Delta\varepsilon_{zz}\approx 1.5\times10^{-3}$, where the z-axis is normal to the film plane [12].

Figure 4 shows a good agreement between the experimental results and model calculations. In spite of similar MCA parameters for (311) and (001) films there is a significant difference between these cases. In (001) films the uniaxial strain ε_{zz} does not tilt $\mathbf{B_{eff}}$ when $\mathbf{B}$ lies in the plane of the film, i.e. $\mathbf{B}\perp$[001]. The tilt of $\mathbf{B_{eff}}$ induced by ε_{zz} in this geometry may take place only due to higher-orders of $\mathbf{m}$ in the magneto-elastic terms [34] or small deviations of the magnetic field from the film plane and the relative contribution of the coherent phonon induced changes of the MCA is much weaker than from non-coherent phonons.

Thus, our analysis shows that in the high-symmetry (001) Galfenol film the coherent phonon mechanism does not influence significantly the magnetization response, and the modulation of the MCA induced by the non-coherent phonons (i.e. temperature rise) is dominant in agreement with previous observations [7-11]. The thermal tilt of $\mathbf{B_{eff}}$ keeps it in the film plane, thus ψ_0 should be close to zero at any B, which is observed experimentally in Fig. 4 (c).

6. Conclusion.

We have studied the precessional response of the magnetization in a film of ferromagnetic metallic Galfenol grown on (311)-GaAs substrate to femtosecond optical excitation. Our experimental results and comparison with theoretical modeling show that in this low-symmetry layer the application of a certain value of magnetic field tunes the dominant mechanism of the excitation between either a pure non-coherent phonon modulation of the magneto-crystalline anisotropy and a coherent phonon mechanism. In particular, the coherent phonon mechanism of ultrafast changes of the MCA may be dominant at high magnetic field B>300 mT applied in the plane of the Galfenol film. The measurements and modeling in the traditional case of a high-symmetry (001) film, confirms exclusively a non-coherent phonon mechanism of the MCA modulation, which is in a good agreement with the previous works in various metal ferromagnetic films.

The work has been supported by the Government of Russia through the program P220 (14.B25.31.0025), the Russian Foundation for Basic Research (15-02-08419) and the Russian Academy of Science. AWR acknowledges support from a Career Acceleration Fellowship (EP/H003487/1), EPSRC, UK.

APPENDIX A. Optical generation of the strain in (311) FeGa film.

The femtosecond laser pulse absorbed by the metal film excites hot electrons near the surface. Their subsequent thermal diffusion and cooling due to the energy transfer to the lattice result in set up of the thermal stress. There are many papers devoted to this problem (see for example, [12,32,33]). Here, we adapt the methodology developed for an isotropic metal film in Ref. [33] to the case of a low-symmetry (311)-FeGa film where elastic anisotropy effects are essential.

The main difference between (311)- and isotropic or high-symmetry oriented films is the optically-induced excitation of two kinds of strain contributions due to the coupling of the thermal stress to two acoustic waves possessing longitudinal displacement components: QLA and QTA ones [25]. It is convenient to introduce two wave amplitudes $u_{0,j}(z,t)$ (j=QLA, QTA) and polarization vectors $\mathbf{e}_j$, which describe the spatial-temporal shape of the displacements as $\mathbf{u}_j(z,t) = \mathbf{e}_j u_{0,j}(z,t)$. The polarization vectors $\mathbf{e}_{\mathrm{QLA}}$=(0.268,0,0.958) and $\mathbf{e}_{\mathrm{QTA}}$=(0.958,0,-0.286) and sound velocities υ_{QLA}= 6.0 km/s and υ_{QTA}= 2.8 km/s in the (311)-FeGa film were obtained from elasticity equations using the elastic constants from Ref. [35]. The corresponding strain components are determined as $\varepsilon_{xz}^{(j)} = \frac{1}{2} e_{j,x} \partial u_{0,j} / \partial z$ and $\varepsilon_{zz}^{(j)} = e_{j,z} \partial u_{0,j} / \partial z$.

To calculate the temperature distribution which determine the thermal stress the two-temperature model is used, which assumes the electrons and the lattice have pseudoequilibrium temperatures T_e and T_i, respectively, and describes both the electron heat conduction and electron-lattice energy relaxation [33]. The temperatures evolution is calculated according to two coupled differential equations:

$$C_e \frac{\partial T_e}{\partial t} = \kappa \frac{\partial^2 T_e}{\partial z^2} - G(T_e - T_i) + P(z,t), \qquad C_i \frac{\partial T_i}{\partial t} = G(T_e - T_i) \tag{A1}$$

where $C_e = A_e T_e$ is the specific electron heat capacity proportional to temperature; $P(z,t) = I(t)(1-R)\alpha \exp(-\alpha z)$ is the absorbed laser power density with intensity time dependence modelled as $I(t) = I_0 \exp(-t^2/\tau_0^2)$. Here τ_0 is laser pulse duration, α^{-1} is the absorption depth, R is light reflection coefficient from the Galfenol surface, κ is the thermal conductivity and G is the electron-phonon coupling constant which are supposed to be temperature independent. Note, that Eq.(A1) neglects the lattice heat conduction in the film, which is usually much less than the electron one. The boundary conditions are $\frac{\partial T_e}{\partial z} = 0$ at z=0 and T_e=T_i=T at z=∞, where T_0 is the initial temperature.

Then the elasticity equations for displacement amplitudes become

$$\rho \frac{\partial^2 u_{0,j}}{\partial t^2} = \rho \upsilon_j^2 \frac{\partial^2 u_{0,j}}{\partial z^2} - e_{j,z} \beta C_i \frac{\partial T_i(z,t)}{\partial z}, \qquad \text{(A2)}$$

where C_i and β are the specific lattice heat capacity and Gruneisen parameter, respectively. The linearized solution of Eqs. (A1-A2) valid for the low laser fluence regime was performed analogously to Ref. [33] for the Fourier components of temperature deviations δT_e and δT_i from the initial temperature and displacement amplitudes:

$$\delta T_e(z,\omega) = \frac{\alpha(1-R)}{\kappa} \frac{I(\omega)}{\alpha^2 - p_T^2} \left[-\exp(-\alpha z) + \frac{\alpha}{p_T} \exp(-p_T z) \right],$$
$$\delta T_i(z,\omega) = \frac{\delta T_e(z,\omega)}{1 - i\omega C_i / G} \qquad \text{(A3)}$$

$$u_{0,j}(z,\omega) = \sigma_j \left\{ \frac{e^{-\alpha z}}{\alpha^2 + k_j^2} - \frac{e^{-p_T z}}{p_T^2 + k_j^2} + \frac{e^{ik_j z}}{2ik_j} \left[\frac{1}{\alpha + ik_j} - \frac{1}{p_T + ik_j} \right] + \frac{e^{-ik_j z}}{2ik_j} \left[-\frac{1}{\alpha - ik_j} + \frac{1}{p_T - ik_j} \right] \right\} +$$
$$+ A_j e^{ik_j z} + B_j e^{-ik_j z}$$

where the introduced parameters are

$$\sigma_j = \frac{e_{j,z}}{\rho \upsilon_j^2} \frac{\beta C_i}{(1 - i\omega C_i / G)} \frac{\alpha^2 (1-R) I(\omega)}{\kappa(\alpha^2 - p_T^2)},$$
$$p_T = \sqrt{\frac{-i\omega C_e}{\kappa} \left(1 + \frac{C_i / C_e}{1 - i\omega C_i / G} \right)}, \qquad k_j = \omega / \upsilon_j \qquad \text{(A4)}$$

where p_T is selected such that $\mathrm{Re}(p_T) > 0$. The constants A_j and B_j are determined from the boundary condition of zero stress at the free surface z=0 and continuity of displacement and stress

components at the (311) FeGa/GaAs interface $z=d$ .One can see from Eq.(A3) that the distribution of temperatures is described by the decaying exponents $\exp(-\alpha z)$ and $\exp(-p_T z)$ and is the smoothly-varying in z function resulting in the time-domain in the fast rise of temperatures followed by slow decay with the characteristic decay time of several nanoseconds. Physically, this corresponds to fast processes of electron heat conduction within the film and quasi-uniform electron-lattice equilibration ($T_e = T_i = T$) which lasts about 10ps that is much less than the typical magnetization precession period and decay time. The mentioned slow decay is due to the heat transfer to the substrate. For the purpose of the magnetization precession consideration occurring for times less than a nanosecond, this time dependence of temperature can be modelled by a step-like change ΔT and the corresponding changes of anisotropy parameters K_1, K_u in Appendix B and in the main text are denoted as $\Delta K_1, \Delta K_u$, respectively.

Moreover, the solution for displacement Fourier amplitudes in Eq.(A3) can be divided into two parts. The first one is a smoothly-varying in z function which analogously to the temperature in the time-domain can be modelled by step-like change of corresponding strain components $\Delta\varepsilon_{xz}^{(j)}$ and $\Delta\varepsilon_{zz}^{(j)}$. The second part describes the QLA and QTA strain pulses, travelling toward and away from the surface. It consists of the terms proportional to exponents $\sim\exp(\pm ik_j z)$ in Eq. (A3). The corresponding strain components in Appendix B are denoted as $\delta\varepsilon_{xz}^{(j)}(z,\omega)$ and $\delta\varepsilon_{zz}^{(j)}(z,\omega)$.

It is important to mention that the true steady state corresponds to the uniform temperature distribution over the lateral direction and isotropic strain which cannot induce magnetization precession. However, relaxation towards this state is very slow and cannot occur faster than time required for acoustic wave propagation along the lateral dimension of the laser excitation spot. In our case, this value exceeds 10 ns and allows us to neglect this process while considering magnetization precession. Mathematically, this corresponds to the use of spatially one-dimensional equations (A1-A3).

For the laser fluence used in the experiment the temperature increase is estimated to be about ΔT =120 K, which justifies the use of the linearized approach. Since some necessary parameters are unknown for Galfenol, we use those of Fe: A_e=672 J/m^{3}K^2 [36], C_i=3.8×10^6 J/m^{3}K, κ=80.4 W/mK, β=1.6 [37]. The electron-phonon coupling constant G=8×10^{17} W/m^{3}K was obtained from Ref. [38] where the electron-phonon relaxation time equal to ~C_e/G was measured to be of 250 fs. Experimentally, we determine $R = 0.6$ and $\alpha^{-1} = 19\text{nm}$. The Galfenol density, ρ, for $x = 19\%$ is estimated to be of 7.95×10^3 kg/m^3. Note, that the quasi-crystalline structure of our

film can decrease the magnetostriction [30], due to decrease of both magnetoelastic and elastic constants, C_{12} first of all, of such a film [35]. In our case, it leads to insignificant changes of the velocities that do not affect our conclusions.

APPENDIX B. Laser-pulse induced magnetization precession.

In general, the fs laser-pulse induced magnetization dynamics are complex processes which include both the precession and demagnetization [1,2]. However, in transitional metals, including iron, the demagnetization occurs on the sub-picosecond timescale, involving complex process of energy exchange between electron, lattice, and spin subsystems as well as angular momentum relaxation [39-41]. In the following, we assume that on this timescale the direction of magnetization does not change, since the typical precession period is in the sub-nanosecond band. This justifies usage of the Landau-Lifshitz equation (2) for treatment of the precession taking the fixed absolute value of magnetization M_S and the free energy density F_M given by Eq.(3).

In Ref. [34] the detailed theory of strain-pulse induced magnetization precession in the ferromagnetic film was developed. We applied here the similar approach allowing additional mechanisms of precession driving by the laser pulse.

It is convenient to analyze precession with the use of spherical angles of magnetization vector, θ and φ. In our case they are introduced for the [311] coordinate system analogously to Ref. [42] (see Fig.1 (a)). The strong demagnetization field B_d and in-plane direction of the external magnetic field $\mathbf{B}$ bring the equilibrium magnetization to the film plane. In this case the precession frequency $\omega_0=2\pi f$ is determined by the standard expression [31]:

$$\omega_0 = \sqrt{a_2 a_1 - a_0^2}, \tag{B1}$$

where introduced parameters $a_1 = \gamma \frac{\partial^2 F_M}{\partial \theta^2}$, $a_2 = \gamma \frac{\partial^2 F_M}{\partial \varphi^2}$, and $a_0 = \gamma \frac{\partial^2 F_M}{\partial \theta \partial \varphi}$ are calculated at equilibrium magnetization orientation $\varphi_0(B)$ and $\theta_0=\pi/2$.

We consider the following two mechanisms inducing perturbation of $\mathbf{B_{eff}}$ caused by coherent and non-coherent phonons. Non-coherent phonons correspond to the film heating and related perturbation of the free-energy parameters while coherent phonons give rise to the coherent strain coupled with the magnetization via inverse magnetostriction. As we show in Appendix A, there are two contributions of coherent phonons with distinct time dependences. The first one can be also modelled by a step-like time dependence of the effective magnetic field. Quantitatively,

the step-like tilt of $\mathbf{B_{eff}}$ induced by both incoherent and coherent phonons can be expressed via variation of the cubic and uniaxial anisotropy parameters ΔK_1 and ΔK_u, and strain components $\Delta\varepsilon_{nz} \equiv \Delta\varepsilon_{nz}^{(QLA)} + \Delta\varepsilon_{nz}^{(QTA)}$, n=x,z (Appendix A), respectively. In the linear-response limit, the simple analytical solution describing the free magnetization precession can be written [34]:

$$\delta m_z(t) = \delta m_0 \sin(\omega_0 t - \psi_0),$$
$$\delta m_0 = \sqrt{\frac{\left(\sum_j Q_\parallel^{(j)} \Delta\xi_j\right)^2}{\omega_0^{\,2}} + \frac{\left(\sum_j a_0 Q_\parallel^{(j)} \Delta\xi_j + a_2 Q_\perp^{(j)} \Delta\xi_j\right)^2}{\omega_0^{\,4}}}, \qquad j = 1,2,3,4,$$
$$\tan\psi_0 = -\frac{\sum_j \left(a_0 Q_\parallel^{(j)} \Delta\xi_j + a_2 Q_\perp^{(j)} \Delta\xi_j\right)}{\omega_0 \sum_i Q_\parallel^{(j)} \Delta\xi_j}, \tag{B2}$$

where $\Delta\xi_j$ represents the magnitude of the step-like deviations of anisotropy parameters K_1, K_u (j=1,2) and strain components ε_{xz}, ε_{zz} (j=3,4), which are denoted as four variables ξ_j. The introduced functions $Q_\parallel^{(j)}, Q_\perp^{(j)}$ are the pulse-induced torques acting on **M** at the in-plane and out of plane tilts of $\mathbf{B_{eff}}$, respectively:

$$Q_\parallel^{(j)} = -\gamma \frac{\partial^2 F_M}{\partial\varphi\partial\xi_j}, \qquad Q_\perp^{(j)} = \gamma \frac{\partial^2 F_M}{\partial\theta\partial\xi_j}. \tag{B3}$$

In compact and simplified form these pulse-induced torques may be written as

$$Q_\parallel^{(1)} = -\gamma \frac{\partial^2 F_M}{\partial\varphi\partial K_1} = -\gamma(1.45 - 3.17\cos^2\varphi)\cos\varphi\sin\varphi,$$
$$Q_\parallel^{(2)} = -\gamma \frac{\partial^2 F_M}{\partial\varphi\partial K_u} = -2\gamma\cos\varphi\sin\varphi,$$
$$Q_\parallel^{(3)} = -\gamma \frac{\partial^2 F_M}{\partial\varphi\partial\varepsilon_{xz}} = -\gamma(-0.21b_2 + 0.42b_1)\cos\varphi\sin\varphi,$$
$$Q_\parallel^{(4)} = -\gamma \frac{\partial^2 F_M}{\partial\varphi\partial\varepsilon_{zz}} = -\gamma(0.13b_2 - 0.26b_1)\cos\varphi\sin\varphi.$$
$$Q_\perp^{(1)} = \gamma \frac{\partial^2 F_M}{\partial\theta\partial K_1} = \gamma(1.15 - 0.98\cos^2\varphi)\cos\varphi,$$
$$Q_\perp^{(2)} = \gamma \frac{\partial^2 F_M}{\partial\theta\partial K_u} = 0,$$
$$Q_\perp^{(3)} = \gamma \frac{\partial^2 F_M}{\partial\theta\partial\varepsilon_{xz}} = \gamma(-0.55b_2 - 0.89b_1)\cos\varphi,$$
$$Q_\perp^{(4)} = \gamma \frac{\partial^2 F_M}{\partial\theta\partial\varepsilon_{zz}} = \gamma(0.56b_1 - 0.28b_2)\cos\varphi, \tag{B4}$$

One can see, that if $\mathbf{B_{eff}}$ is aligned along *x*-axis (φ=0) or *y*-axis (φ=π/2) $Q_{\parallel}^{(j)} = 0$ for all contributions: neither temperature changes of the anisotropy coefficients nor strain induce the in-plane tilt of $\mathbf{B_{eff}}$. Optical excitation gives rise, in general, to the out-of-plane tilt of $\mathbf{B_{eff}}$, excepting its in-plane orientation along *y*-axis. At $\varphi \approx 0$ the K_1-related torque $Q_{\perp}^{(1)}$ has minimum absolute value, while the strain-related ones $Q_{\perp}^{(3)}$ and $Q_{\perp}^{(4)}$ reach their maxima. Thus, at $\mathbf{B_{eff}} \parallel$ [-233] direction the contribution of coherent phonons becomes dominating.

The other coherent phonon mechanism of the precession excitation is QLA and QTA strain pulses. Their amplitude and time evolution are calculated in Appendix A. The resulting amplitudes of the free magnetization precession can be determined analogously to Ref. [34]:

$$\delta m_0(z) = \left| \left(-i\frac{a_2}{\omega_0} Q_{\perp}^{(3)} - \left(i\frac{a_0}{\omega_0} - 1 \right) Q_{\parallel}^{(3)} \right) \delta\varepsilon_{xz} + \left(-i\frac{a_2}{\omega_0} Q_{\perp}^{(4)} - \left(i\frac{a_0}{\omega_0} - 1 \right) Q_{\parallel}^{(4)} \right) \delta\varepsilon_{zz} \right|, \tag{B5}$$

where $\delta\varepsilon_{nz} \equiv \delta\varepsilon_{nz}^{(QLA)}(z,\omega_0) + \delta\varepsilon_{nz}^{(QTA)}(z,\omega_0),\ n = x,z$ are the strain Fourier components at precession frequency ω_0. Note that in Eq. (B5) both QLA and QTA strain pulse contributions are taken into account (see Appendix A for details). The numerical calculations show that the strain pulses perturb the magnetic system much weaker than the step-like strain components. Therefore, strain-pulses contribution is not discussed in the main text of the paper.

In the actual experiment, probing of the magnetization at a certain coordinate z is impossible. The experimental signal reflects the time evolution of the magnetization averaged over the layer thickness taking into account the properties of the probe light pulse, in our case the finite absorption depth of light. Thus, we calculate the mean precession amplitude as $\overline{\delta m_z} = \alpha \int_0^d e^{-\alpha z} \delta m_0(z) dz$, where α^{-1} is the probe absorption depth and d is film thickness.

REFERENCES

[1] E. Beaurepaire, J.-C. Merle, A. Daunois, and J.-Y. Bigot, Ultrafast Spin Dynamics in Ferromagnetic Nickel, Phys. Rev. Lett. **76**, 4250 (1996).

[2] A. Kirilyuk, A. V. Kimel, and T. Rasing, Ultrafast optical manipulation of magnetic order, Rev. Mod. Phys. **82**, 2731 (2010).

[3] M. H. Kryder, E. C. Gage, T. W. McDaniel, W. A. Challener, R. E. Rottmayer, G. Ju, Y.-T. Hsia, and M. F. Erden, Heat assisted magnetic recording, Proc. IEEE **96**, 1810 (2008).

[4] T. A. Ostler, J. Barker, R. F. L. Evans, R. W. Chantrell, U. Atxitia, O. Chubykalo-Fesenko, S. El Moussaoui, L. Le Guyader, E. Mengotti, L. J. Heyderman, F. Nolting, A. Tsukamoto, A. Itoh, D. Afanasiev, B. A. Ivanov, A. M. Kalashnikova, K. Vahaplar, J. Mentink, A. Kirilyuk, Th. Rasing, and A.V. Kimel. Ultrafast heating as a sufficient stimulus for magnetization reversal in a ferrimagnet, Nature Commun. **3**, 666 (2012).

[5] S. Mangin, M. Gottwald, C-H. Lambert, D. Steil, V. Uhlir, L. Pang, M. Hehn, S. Alebrand, M. Cinchetti, G. Malinowski, Y. Fainman, M. Aeschlimann and E. E. Fullerton, Engineered materials for all-optical helicity-dependent magnetic switching, Nature Mater. **13**, 286 (2014).

[6] W. K. Hiebert, A. Stankiewicz, and M. R. Freeman, Direct Observation of Magnetic Relaxation in a Small Permalloy Disk by Time-Resolved Scanning Kerr Microscopy, Phys. Rev. Lett. **79**, 1134 (1997).

[7] J.-Y. Bigot*, M. Vomir, L.H.F. Andrade, E. Beaurepaire, Ultrafast magnetization dynamics in ferromagnetic cobalt: The role of the anisotropy, J. Chem. Phys. **318**, 137 (2005).

[8] A. A. Rzhevsky, B. B. Krichevtsov, D. E. Bürgler, and C. M. Schneider, Magnetization dynamics induced by ultrashort optical pulses in Fe/Cr thin films, Phys. Rev. B **75**, 224434 (2007).

[9] E. Carpene, E. Mancini, D. Dazzi, C. Dallera, E. Puppin, and S. De Silvestri, Ultrafast three-dimensional magnetization precession and magnetic anisotropy of a photoexcited thin film of iron, Phys. Rev. B **81**, 060415 (2010).

[10] J. Kisielewski, A. Kirilyuk, A. Stupakiewicz, A. Maziewski, A. Kimel, Th. Rasing, L. T. Baczewski, and A. Wawro, Laser-induced manipulation of magnetic anisotropy and magnetization precession in an ultrathin cobalt wedge, Phys. Rev. B **85**, 184429 (2012)

[11] T. P. Ma, S. F. Zhang, Y. Yang, Z. H. Chen, H. B. Zhao, and Y. Z. Wu, Distinguishing the laser-induced spin precession excitation mechanism in Fe/MgO(001) through field orientation dependent measurements, J. Appl. Phys. **117**, 013903 (2015).

[12] C. Thomsen, H. T. Grahn, H. J. Maris, and J. Tauc, Surface generation and detection of phonons by picosecond light pulses, Phys. Rev. B **34**, 4129 (1986).

[13] H. B. Zhao, D. Talbayev, Q. G. Yang, and G. Lüpkea, A. T. Hanbicki, C. H. Li, O. M. J. van ’t Erve, G. Kioseoglou, and B. T. Jonker, Ultrafast magnetization dynamics of epitaxial Fe films on AlGaAs (001), Appl. Phys. Lett. **86**, 152512 (2005).

[14] J.-W. Kim, M. Vomir, and J.-Y. Bigot, Ultrafast Magnetoacoustics in Nickel Films, Phys. Rev. Lett. **109**, 166601 (2012).

[15] J. V. Jäger, A. V. Scherbakov, T. L. Linnik, D. R. Yakovlev, M. Wang, P. Wadley, V. Holy, S. A. Cavill, A. V. Akimov, A. W. Rushforth, and M. Bayer. Picosecond inverse magnetostriction in galfenol thin films. Appl. Phys. Lett. **103**, 032409 (2013).

[16] Y. Yahagi, B. Harteneck, S. Cabrini, and H. Schmidt, Phys. Rev. B **90**, 140405(R) (2014).

[17] J. Janušonis, C. L. Chang, P. H. M. van Loosdrecht, and R. I. Tobey, Appl. Phys. Lett. **106**, 181601 (2015).

[18] M. van Kampen, C. Jozsa, J. T. Kohlhepp, P. LeClair, L. Lagae, W. J. M. de Jonge, and B. Koopmans, All-Optical Probe of Coherent Spin Waves, Phys. Rev. Lett. **88**, 227201 (2002).

[19] M. Vomir, L. H. F. Andrade, L. Guidoni, E. Beaurepaire, and J.-Y.Bigot, Real Space Trajectory of the Ultrafast Magnetization Dynamics in Ferromagnetic Metals, Phys. Rev. Lett. **94**, 237601 (2005).

[20] J. Atulasimha and A. B. Flatau, A review of magnetostrictive iron–gallium alloys, Smart Mater. Struct. **20**, 043001 (2011).

[21] D. E. Parkes, L. R. Shelford, P. Wadley, V. Holý, M. Wang, A. T. Hindmarch, G. van der Laan, R. P. Campion, K. W. Edmonds, S. A. Cavill, and A. W. Rushforth, Magnetostrictive thin films for microwave spintronics, Sci. Reports **3**, 2220 (2013).

[22] D. E. Parkes, S. A. Cavill, A. T. Hindmarch, P. Wadley, F. McGee, C. R. Staddon, K. W. Edmonds, R. P. Campion, B. L. Gallagher, and A. W. Rushforth, Non-volatile voltage control of magnetization and magnetic domain walls in magnetostrictive epitaxial thin films, Appl. Phys. Lett. **101**, 072402 (2012).

[23] A. E. Clark, M. Wun-Fogle, J. B. Restorff, K. W. Dennis, T. A. Lograsso, and R. W. McCallum, Temperature dependence of the magnetic anisotropy and magnetostriction of Fe100−xGax (x=8.6, 16.6, 28.5), J. of Appl. Phys. **97**, 10M316 (2005).

[24] C. Thomsen, H. T. Grahn, H. J. Maris, and J. Tauc, "Picosecond interferometric technique for study of phonons in the brillouin frequency range," Optics Commun. **60** (1,2), 55-58 (1986).

[25] A. V. Scherbakov, M. Bombeck, J.V. Jäger, A.S. Salasyuk, T.L. Linnik, V.E. Gusev, D.R. Yakovlev, A.V. Akimov, and M. Bayer, Picosecond opto-acoustic interferometry and polarimetry in high-index GaAs, Optic Express **21**, 16473 (2013).

[26] L. D. Landau, E. M. Lifshitz and L. P. Pitaevskii, Electrodynamics of continuous media (Pergamon, London, 1984).

[27] J. W. Tucker and V. W. Rampton, Microwave ultrasonics in solid state physics (North-Holland, Amsterdam, 1972).

[28] S. Blundell, Magnetism in condensed Matter (Oxford University Press, Oxford, 2001).

[29] J.B.Restorff, M.Wun-Fogle, K.B.Hathaway, A.E.Clark, T.A.Lograsso, and G.Petculescu, Tetragonal magnetostriction and magnetoelastic coupling in Fe-Al, Fe-Ga, Fe-Ge, Fe-Si, Fe-Ga-Al, and Fe-Ga-Ge alloys, J. of Appl. Phys. **111**, 023905 (2012).

[30] J. Atulasimha, A. B. Flatau, and E. Summers, Characterization and energy-based model of the magnetomechanical behavior of polycrystalline iron–gallium alloys, Smart Mater. Struct. **16**, 1265 (2007).

[31] G.V. Skrotskii, L.V. Kurbatov, Phenomenological Theory of Ferromagnetic Resonance, in Ferromagnetic Resonance edt. S. V. Vonsovskii (Pergamon, Paris, 1966), pp. 12-77.

[32] G. Tas and H. J. Maris, Electron diffusion in metals studied by picosecond ultrasonics, Phys. Rev. B **49**, 15046 (1994).

[33] O. B. Wright and V. E. Gusev, Ultrafast generation of acoustic waves in copper, IEEE Trans. Ultrason. Ferroelectr. Freq. Control. **42**, 331 (1995).

[34] T. L. Linnik, A. V. Scherbakov, D. R. Yakovlev, X. Liu, J. K. Furdyna, and M. Bayer, Theory of magnetization precession induced by a picosecond strain pulse in ferromagnetic semiconductor (Ga,Mn)As, Phys. Rev. B **84**, 214432 (2011).

[35] A. E. Clark, K. B. Hathaway, M. Wun-Fogle, J. B. Restorff, T. A. Lograsso, V. M. Keppens, G. Petculescu, and R. A. Taylor, Extraordinary magnetoelasticity and lattice softening in bcc Fe-Ga alloys, J. of Appl. Phys. **93**, 8621 (2003).

[36] A. Tari, *The Specific Heat of Matter at Low Temperatures* (London: Imperial College Press, 2003), p. 71.

[37] David R. Lide, *CRC Handbook of Chemistry and Physics* (CRC Press, Florida, 2003), p. ??.

[38] E. Carpene, E. Mancini, C. Dallera, M. Brenna, E. Puppin and S. De Silvestri, Dynamics of electron-magnon interaction and ultrafast demagnetization in thin iron films, Phys. Rev. B **78**, 174422 (2008).

[39] M. Djordjevic, M. Lüttich, P. Moschkau, P. Guderian, T. Kampfrath, R. G. Ulbrich, M. Münzenberg, W. Felsch, and J. S. Moodera, Comprehensive view on ultrafast dynamics of ferromagnetic films, Phys. Status Solidi C **3**, 1347 (2006).

[40] U. Atxitia, O. Chubykalo-Fesenko, J. Walowski, A. Mann, and M. Munzenberg, Evidence for thermal mechanisms in laser-induced femtosecond spin dynamics, Phys. Rev. B **81**, 174401 (2010).

[41] B. Koopmans, G. Malinowski, F. Dalla Longa, D. Steiauf, M. Fahnle, T. Roth, M. Cinchetti, and M. Aeschlimann, Explaining the paradoxical diversity of ultrafast laser-induced demagnetization, Nature Mater. **9**, 259 (2010).

[42] M. Bombeck, J. V. Jager, A. V. Scherbakov, T. Linnik, D. R. Yakovlev, X. Liu, J. K. Furdyna, A. V. Akimov, and M. Bayer, Magnetization precession induced by quasitransverse picosecond strain pulses in (311) ferromagnetic (Ga,Mn)As, Phys. Rev. B **87**, 060302(R) (2013).

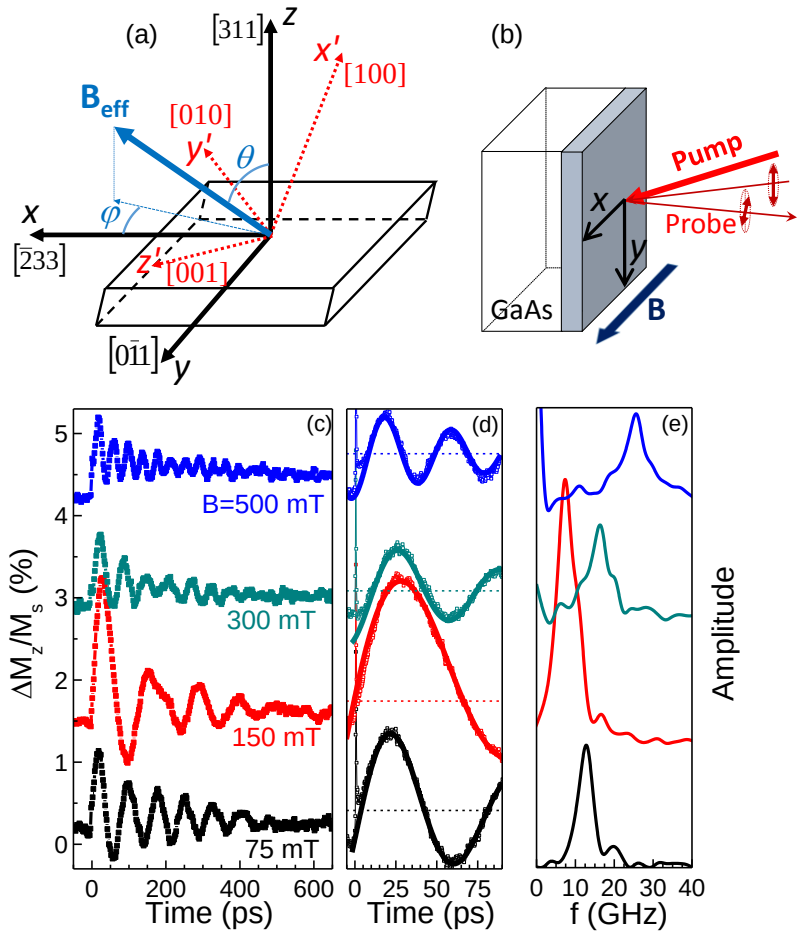

Figure 1. (a) The coordinate system of the studied (311)-Galfenol film describing the experimental geometry. (b) Experimental scheme. (c) , (d) The TRMOKE signals for four values of external magnetic field *B* measured at *P*=10 mJ/cm^2 with low (c) and high (d) temporal resolutions. (e) The spectra obtained as FFT of the TRMOKE signals shown in (c).

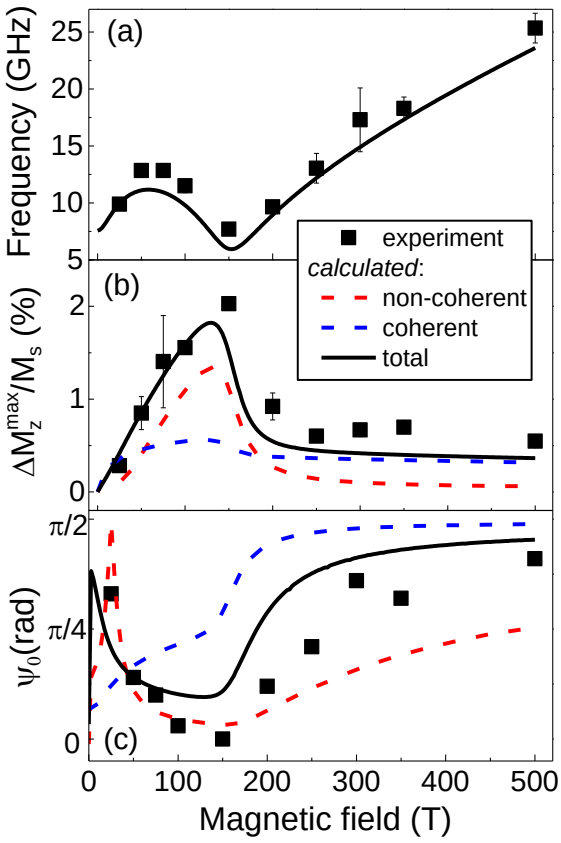

Figure 2. Experimental (symbols) and calculated (lines) magnetic field dependences of the precession frequency (a), amplitude (b) and initial phase (c) for (311)-Galfenol film. The experimental dependence of frequency and amplitude are averaged values obtained by two methods: FFT analysis of the temporal curves and the fit by Eq. (1). The error bars show the difference between the values obtained by different methods if it exceeds the symbol size. The dashed lines show the dependences calculated separately for non-coherent (red lines) or coherent (blue lines) mechanisms, respectively.

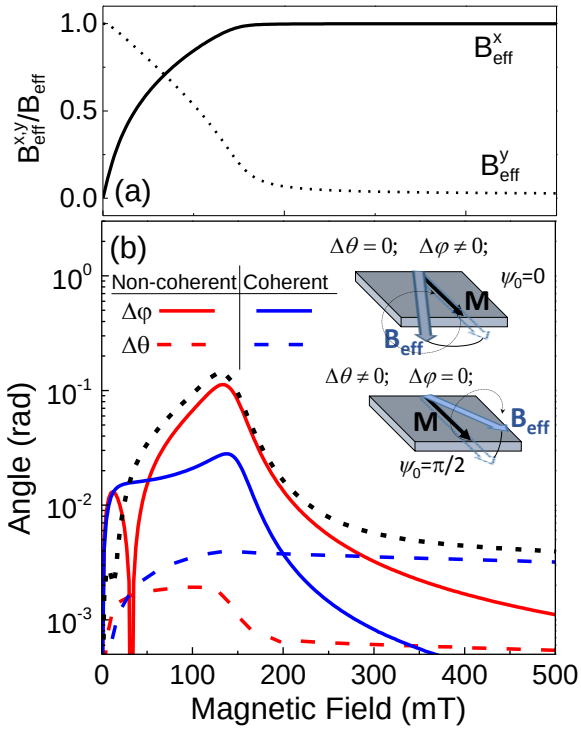

Figure 3. (a) The magnetic field dependences of *x* (solid line) and *y* (dashes line) projection of the equilibrium in-plane orientation of the effective field **B**$_{eff}$. (b) The field dependences of the **B**$_{eff}$ tilt angles $\Delta\varphi$ (solid lines) and $\Delta\theta$ (dashed lines) under the pulsed optical excitation resulting in the increase of temperature on 50 K. The red and blue lines show the calculation results when only non-coherent or coherent phonon mechanisms are taken into account respectively. Short-dashed line shows the net tilt of **B**$_{eff}$, $\eta = \sqrt{\Delta\varphi^2 + \Delta\theta^2}$, induced by both mechanisms. The upper and lower insets show two cases of purely in-plane and out-of-plane tilts of **B**$_{eff}$ respectively.

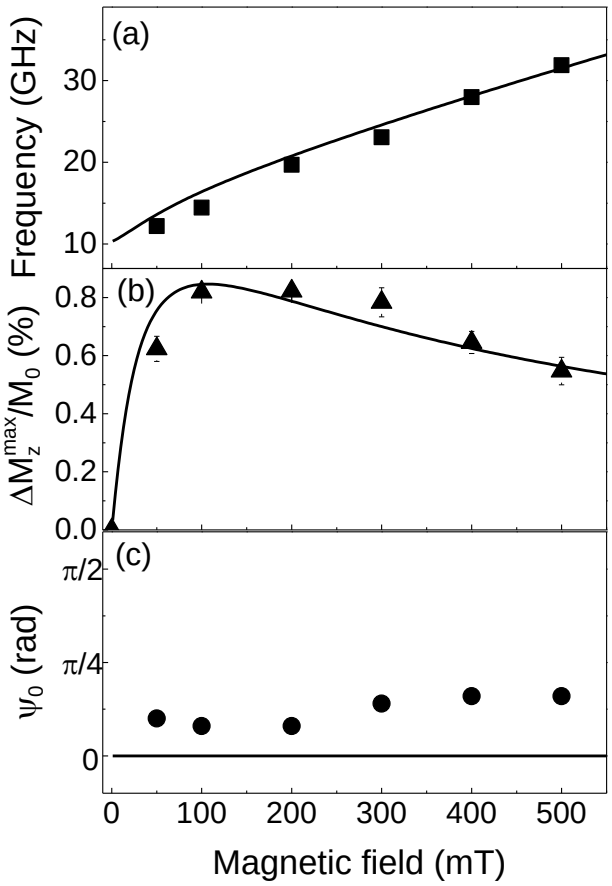

Figure 4. The measured (symbols) and calculated (solid lines) magnetic field dependences of the precession frequency (a), amplitude (b), and initial phase (c) in the high-symmetry (100)- Galfenol film.